JOURNAL OF APPLIED ELECTROCHEMISTRY 21 (1991) 816–823

Kinetics and mechanism of the electroreduction of anodic layers produced on cadmium in alkaline solution containing sodium sulphide

L. M. GASSA, S. B. SAIDMAN*, J. R. VILCHE, A. J. ARVIA‡

Instituto de Investigaciones Fisicoquímicas Teóricas y Aplicadas (INIFTA), Facultad de Ciencias Exactas, Universidad Nacional de La Plata, Sucursal 4, Casilla de Correo 16, 1900 La Plata, Argentina

Received 12 July 1990; revised 18 January 1991

The kinetics of the potentiostatic electroreduction of different anodic layers produced on cadmium in Na_2S containing alkaline solutions has been studied at 25° C. Two types of anodic layer were used: (i) layers produced in the potential range of CdS and $Cd(OH)_2$ stability, and (ii) layers predominantly composed of CdS. The electroreduction kinetics for both layers can be explained reasonably well throughout the nucleation and growth processes under diffusion control.

1. Introduction

There are a number of studies on semiconductor photoelectrodes, such as cadmium sulphide, focusing on the charge transfer kinetic processes related to solar energy conversion, water splitting, chemical sensors and imaging and memory devices [1–6]. However, in the case of cadmium sulphide there is a limitation to its use because of the cost and difficulty of preparing single crystals on a large scale [7, 8]. Primarily for these reasons, electrochemical methods of preparation of polycrystalline CdS films have been investigated.

The anodic layers produced on cadmium in alkaline solutions containing sodium sulphide may be composed of either CdS or $Cd(OH)_2$ as main product depending on both the OH^-/sulphide ion concentration ratio in solution [9–13] and the applied electric potential. The formation of $Cd(OH)_2$ layers at high pH involves the simultaneous formation of soluble Cd^{2+} species.

The kinetics of anodic CdS layer growth on polycrystalline Cd in sulphide containing solutions at pH 14 was interpreted as a multiple stage process [10], the initial stage involving the activation controlled deposition of one half a CdS monolayer, followed by a place exchange reaction involving Cd^{2+} and S^{2-} ions, which opens the possibility of a second one half monolayer of CdS to be formed. Further growth of the CdS layer produces a thick, either porous or polycrystalline, CdS layer [10, 12]. The electroreduction kinetics of the different CdS layers is also a complex process [9–13]. The voltammetric electroreduction of CdS layers allows the delineation of the potential ranges where different processes take place, particularly when the anodic layer has various constituents such as CdS and $Cd(OH)_2$ [13]. This opens the possibility of investigating further the electroreduction of CdS layers by using appropriate potential routines and following the kinetics of the electroreduction reaction under a constant potential in order to determine to what extent the kinetics of this reaction follows a nucleation and growth type mechanism. This analysis provides a new insight about the probable mechanisms of the electroreduction reactions of anodic layers produced on cadmium in alkaline solutions containing sodium sulphide.

2. Experimental details

The experimental setup was described in previous publications [13–15]. "Specpure" cadmium discs (Johnson Matthey Chemicals Ltd., 0.30 cm^2 apparent area) embedded in PTFE holders were used as working electrodes in 0.01 M NaOH + 0.01 M Na_2S at 25° C, under purified nitrogen gas saturation. The electrolyte solution was prepared from p.a. Merck reagents and triply-distilled water, and it was carefully deareated prior to the addition of sodium sulphide. Cadmium electrodes were mechanically polished with 400 and 600 grade emergy papers and 1 μm and 0.3 μm grit alumina-acetone suspensions, and then thoroughly rinsed in triply-distilled water. Potentials were measured against a SCE properly shielded, but in the text they are referred to the NHE scale.

Two types (I and II) of experiments were made. Type I-experiments consisted firstly of a 5 min cathodization at − 1.76 V, i.e. in the HER potential range to achieve a reproducible electroreduced Cd surface. Subsequently, the electrode was subjected to either a single (STPS) or repetitive (RTPS) triangular potential sweeps which were applied at convenience between

* Present address: Laboratorio de Electroquímica, Universidad Nacional del Sur, Bahía Blanca, Argentina.
‡ Author to whom all correspondence should be addressed.

0021-891X/91 $03.00 + .12

cathodic ($E_{s,c} = -1.76$ V) and anodic (-0.86 V $\leqslant E_{s,a} \leqslant -0.26$ V) switching potentials at a scan rate, $v = 0.1\,V\,s^{-1}$.

Type II-experiments combined linear potential scans with potential steps, usually two potential steps, covering different preset potential regions. The first potential step (E_i) was applied for a certain time (τ), to modify the anodic layer in a preestablished way, i.e. to change the total amount of anodic product, and to produce ageing effects in order to vary the ratio of the anodic layer constituents. The second potential step (E_f) was set sufficiently negative to electroreduce the anodic layer, the corresponding current transients being systematically recorded. (E_f) was set in the -1.38 V to -1.73 V range. For the sake of clarity, the potential routines are displayed as insets in the graphs.

3. Results and interpretation

3.1. *Voltammetric data*

The voltammograms of Cd in 0.01 M NaOH + 0.01 M Na_2S at $v = 0.1 V\,s^{-1}$ (Fig. 1) show a pair of conjugated peaks (A and B). The initiation of the anodic peak A coincides with the thermodynamic threshold potential of the $Cd/CdS/S^{2-}$ electrode, E_r (10^{-2} M Na_2S) $= -1.136$ V [16], and the location and the charge of the cathodic peak B depends strongly on $E_{s,a}$. In addition the voltammograms also show an anodic current contribution due to the formation of a cadmium hydroxide-oxide layer at potentials more positive than that of peak A, and a cathodic current contribution due to the electroredution of the anodic layer. The detailed analysis of these voltammograms has been given elsewhere [13]. At present the voltammograms are presented with the purpose of describing the potential ranges of the different reactions.

3.2. *Electroreduction current transients*

3.2.1. Relatively thick CdS layers. For Cd electrodes covered with a cadmium sulphide layer formed by potential cycling between $E_{s,c} = -1.76$ V and $E_{s,a} = -0.26$ V at $v = 0.1\,V\,s^{-1}$ (Fig. 1a), the potentiostatic electroreduction current transients of the process related to peak B was studied at values of E_f ranging from -1.38 to -1.73 V. In this case the electroreduction process at E_f was preceded by a potential step at either $E_i = -1.26$ V for $\tau = 3$ s (Fig. 2) or at $E_i = -0.96$ V for $\tau = 3$ min (Fig. 3). At $E_i = -1.26$ V the anodic layer remaining on the electrode surface consisted of a few layers of CdS, as can be derived from the charge of the cathodic current transients after correction for the HER baseline. Otherwise, at $E_i = -0.96$ V the anodic layer resulting after $\tau = 3$ min is probably not yet completely free of $Cd(OH)_2$ species, and the main product formed at E_i, is the anionic form of Cd resulting from the high local pH. The initial build-up of these current transients includes the double layer charging which cannot be depicted in the time scale of the figure. The rise time estimated from the RC value is 10^{-5} s.

At $E_i = -1.26$ V the cathodic current transients (Fig. 2) show, for $E_f < 1.54$ V, a small minimum current density, j_m at the time t_m, and a peaked current density value, j_M at the time t_M. The value of j_M increases and that of t_M decreases as E_f is set more negatively. These current transients appear to be the sum of a continuous current decay and a peaked-value current function, as is usually found in nucleation and growth rate controlled processes.

The complex nature of the current transients can be better seen through Type II experiments for $E_i = -0.96$ V (Fig. 3). In this case the initial current decay is observed at any E_f value and its influence on the rest of the transient becomes greater as E_i is set more negatively. The initial falling part of the current density transients exhibits a linear j against $t^{-1/2}$ relationship for $t < 10$ ms. In these cases both the slope of the straight lines and the value of the ordinate extrapolated to $t \longrightarrow \infty$, increase as E_f is moved negatively (Fig. 4). These results suggest that there is a diffusion contribution in the potentiostatic electroreduction of the anodic layer. Likewise, the extrapolation of the j

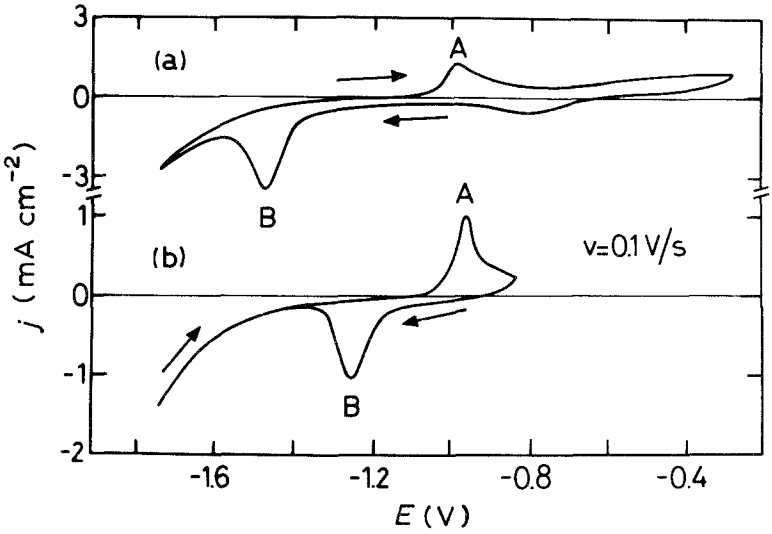

Fig. 1. Voltammograms run at $v = 0.1\,V\,s^{-1}$ for Cd in 0.01 M NaOH + 0.01 M Na_2S between $E_{s,c} = -1.76$ V and different $E_{s,a}$. (a) $E_{s,a} = -0.26$ V; (b) $E_{s,a} = -0.86$ V.

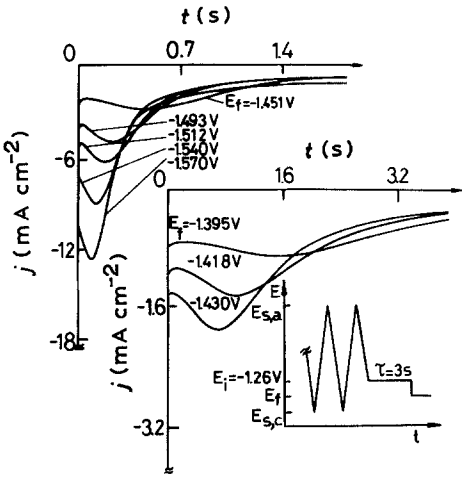

Fig. 2. Cathodic current transients recorded at different E_f after a potential holding at $E_i = -1.26\,V$ for $\tau = 3\,s$. The electrode has been previously cycled at $v = 0.1\,V\,s^{-1}$ between $E_{s,c} = -1.76\,V$ and $E_{s,a} = -0.26\,V$.

against $t^{-1/2}$ plots (Fig. 4) at $t \to \infty$ gives a limiting current which becomes slightly higher than the baseline current read in the voltammogram at E_f (Fig. 1a). Therefore, these results allowed the distinguishing of two contributions in the electroreduction reaction, which overlap extensively in the decay process (Figs 2 and 3). The results of data processing are seen in Fig. 5. The j/j_M against t/t_M plots fit the single layer equation corresponding to an instantaneous nucleation 2D growth model [17–19]. Furthermore, it is interesting to note that the experimental values of $Q_M/j_M t_M$ for both types of experiments are 0.68 ± 0.04, in agreement with the value derived from the above mentioned 2D growth model which is 0.648 [20].

On the other hand, when $E_{s,a}$ is more positive, i.e. $E_{s,a} = 0.16\,V$, and E_i is set at a relatively large negative potential, i.e. $E_i = -1.36\,V$ (Fig. 5) the shape of the current transient can be fitted according to a j^2/j_M^2 against t/t_M plot, which corresponds to 3D

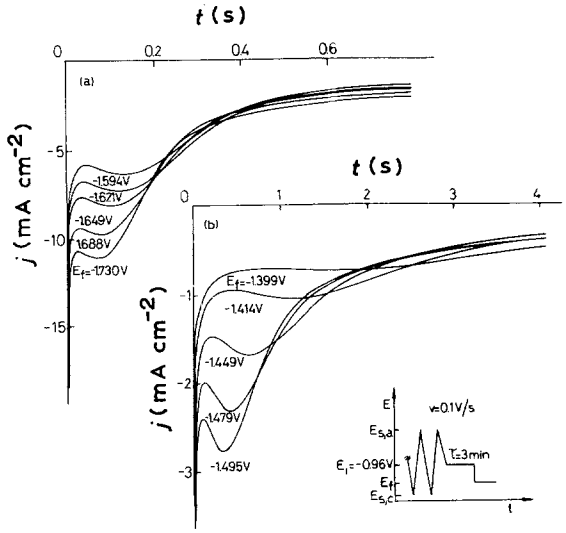

Fig. 3. Cathodic current transients recorded at different E_f after a potential holding at $E_i = -0.96\,V$ for $\tau = 3\,min$. The electrode has been previously cycled at $v = 0.1\,V\,s^{-1}$ between $E_{s,c} = -1.76\,V$ and $E_{s,a} = -0.26\,V$.

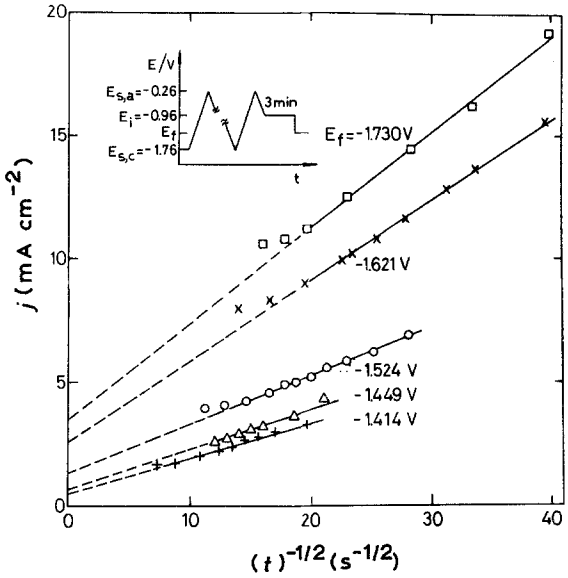

Fig. 4. Plot of j against $t^{-1/2}$ for the initial falling part of the cathodic current transients run at different E_f after a potential holding at $E_i = -0.96\,V$ for $\tau = 3\,min$. The electrode has been previously cycled at $v = 0.1\,V\,s^{-1}$ between $E_{s,c} = -1.76\,V$ and $E_{s,a} = -0.26\,V$.

multiple instantaneous nucleation with diffusion controlled growth [21].

3.2.2. Thin CdS layers. Thin CdS layers are anodically prepared under the conditions illustrated in Fig. 1b, i.e., by setting $E_{s,a}$ at $-0.86\,V$ to avoid the potential range where oxygen-containing species are produced. Furthermore, before the potentiostatic electroreduction to those CdS layers, they were aged for $\tau = 3\,s$ either at $-1.16\,V$ (Fig. 7a) or at $-1.06\,V$ (Fig. 7b). During this time, however, it is possible that a part of the CdS layer disappears. The latter effect probably increases as the value of E_i goes negative (Fig. 8). It should also be noticed that the ageing processes occurring at E_i should depend on τ, although this influence for the purpose of the present work can be discarded.

The electroreduction current transients obtained for thin CdS layers under constant potential conditions (Figs 7 and 8) decay monotonically, but as E_f is moved negatively, they approach an initial current density plateau, j_{lim}, the extension of the latter increasing, and the height decreasing, proportionally to the applied potential step. The rest of the current transients show a smooth sigmoid form, involving a relatively extended linear j/t relationship in the vicinity of the inflection point. The slopes of these straightline portions become directly proportional to the applied overvoltage, the latter defined with respect to the reversible potential of the Cd/CdS/(xM)S^{2-} electrode. It is also interesting to note that the CdS potentiostatic electroreduction process at these layer thicknesses levels depends considerably on the preceding electrode treatment at E_i (Fig. 8). The potential holding at E_i does not produce any increase in charge but causes a big change in the rate of the electroreduction process. This is an indication that ageing causes remarkable

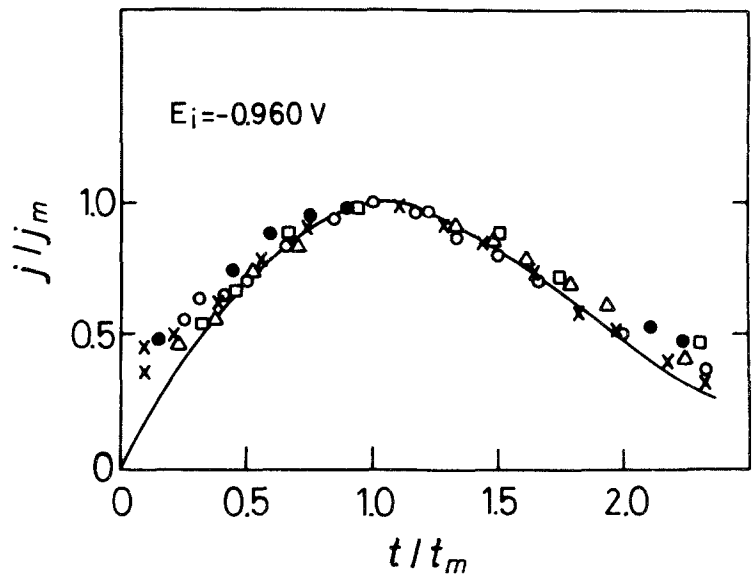

Fig. 5. Comparison of j/j_m against t/t_m plots. Instantaneous nucleation and 2D growth equation (full lines). Points are taken from current transients run at different E_f after correction for the contribution indicated in Fig. 4. The potential-time programme is the same depicted in Fig. 3. E_f: (○) −1.1414, (△) −1.449, (×) −1.524, (●) −1.621 and (□) −1.730 V.

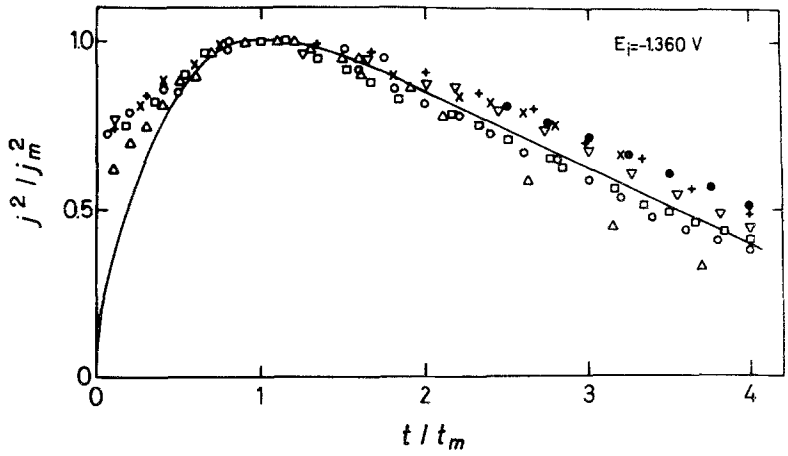

Fig. 6. Comparison of j^2/j_m^2 against t/t_m plots. Instantaneous nucleation and 3D growth (full line). Points are taken from the current transients run at different E_f after a potential holding at $E_i = -1.36$ V for $\tau = 3$ s. The electrodes were previously cycled at $v = 0.1\,V\,s^{-1}$ between $E_{s,c} = -1.76$ V and $E_{s,a} = -0.16$ V. E_f: (○) −1.384, (□) −1.397, (△) −1.415, (○) −1.473, (×) −1.544, (▽) −1.560 and (+) −1.581 V.

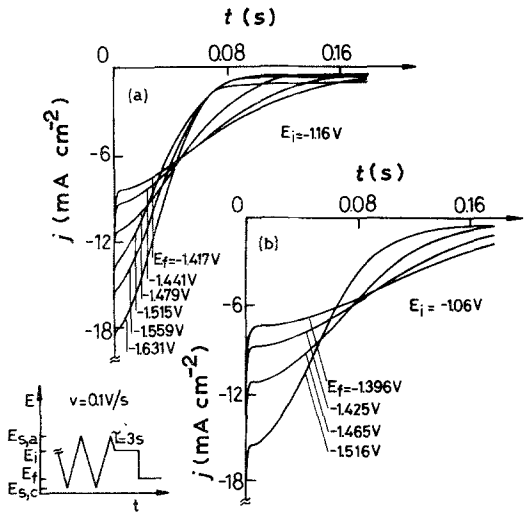

Fig. 7. Influence of E_i on the current transients recorded at different E_f after a potential holding at E_i for $\tau = 3$ s. The electrodes were previously cycled at $v = 0.1\,V\,s^{-1}$ between $E_{s,c} = -1.76$ V and $E_{s,a} = -0.86$ V. (a) $E_i = -1.16$ V; (b) $E_i = -1.06$ V.

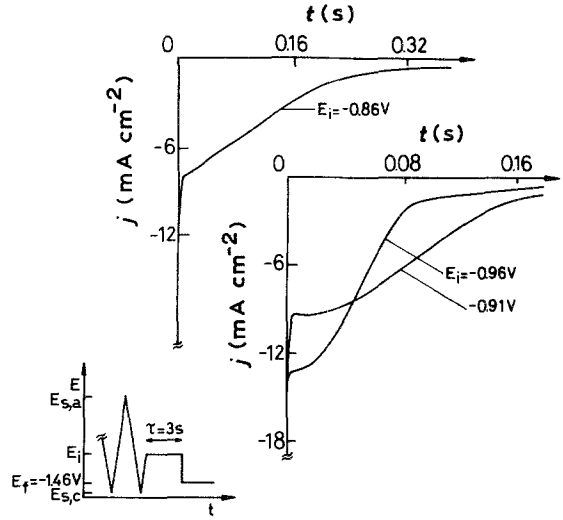

Fig. 8. Influence of E_i on the current transients recorded at $E_f = -1.46$ V after a potential holding at E_i for $\tau = 3$ s. The electrodes were previously cycled at $v = 0.1\,V\,s^{-1}$ between $E_{s,c} = -1.76$ V and $E_{s,a} = -0.86$ V.

changes in the structure of the anodic layer at the monolayer level.

4. Discussion

4.1. *Thick anodic layer electroreduction mechanism*

The anodization of Cd in Na_2S containing alkaline solutions produces a complex layer whose composition varies from that of CdS to that of CdS + $Cd(OH)_2$ depending on the voltammetric switching potentials and solution composition [13–15]. The potential stepping at E_i values in different regions of the voltammogram allows separation of the various contributions to the global electroreduction process.

The anodic layers formed by potential cycling up to -0.26 V involve two main constituents, namely, CdS and $Cd(OH)_2$ containing species. When these layers are held at E_i either -1.26 V for 3 s (Fig. 2) or -0.96 V for 3 min (Fig. 3) the Cd oxide-hydroxide species can be electroreduced and the remaining surface layer is principally related to CdS species. Under these conditions the cathodic current transients, $j(t)$, can be satisfactorily reproduced as the sum of two processes, the corresponding instantaneous contributions being denoted as $j_1(t)$ and $j_2(t)$:

$$j(t) = j_1(t) + j_2(t) \quad (1)$$

where

$$j_1(t) = P_1 t \exp(-P_2 t^2) \quad (2)$$

and

$$j_2(t) = P_3 \exp(-P_4 t) \quad (3)$$

Equation 2 corresponds to the current decay of a 2D nucleation and growth process under instantaneous nucleation and charge transfer control [18]. In this case,

$$P_1 = \frac{2zF\pi hMk^2N_0}{\rho} \quad (4)$$

and

$$P_2 = \frac{\pi M^2 k^2 N_0}{\rho^2} \quad (5)$$

where M is the molecular weight of CdS, k is the rate constant for crystal growth parallel to the surface, ρ is the density of the surface layer, and h is the height of the growing layer, when N_0 nuclei are instantaneously formed. Figures 9 and 10 show the good agreement between experimental and calculated data, the latter calculated from Equation 1 with the set of parameters assembled in Table 1. The potential dependencies of P_1 and P_2 are shown in Fig. 11. At the lowest E_f values both P_1 and P_2 tend to be nearly potential independent, but for $E_f > -1.58$ V, the $\log P_i$ ($i = 1, 2$) against E_f plots, approach slopes in the 0.06–0.07 V decade^{-1} range.

Equation 3, which represents the initial falling current transient corrected for the electrical double layer discharge, can be assigned to the electroreduction of the inner part of the anodic layer in contact with the electrode. The values of P_3 and P_4 change linearly with potential (as will be shown later), and they have to be interpreted through a model. In principle, Equation 3 can be related to an instantaneous nucleation and 2D growth under diffusion control [22]. In this case P_3 and

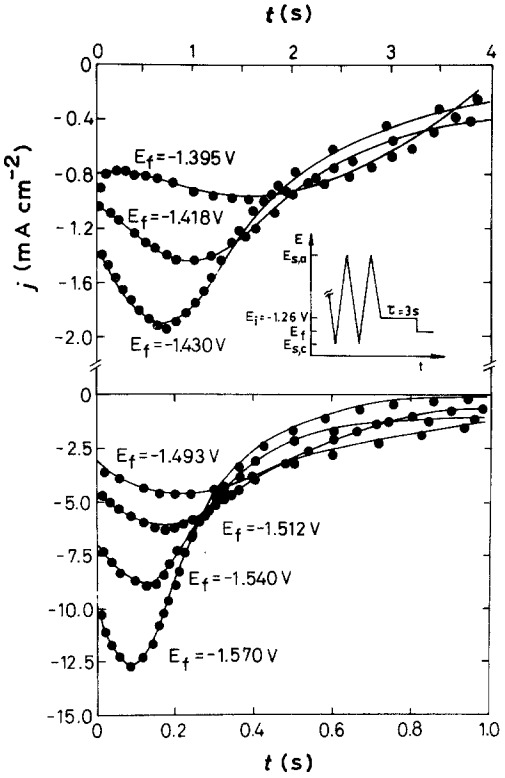

Fig. 9. Fitting of current transient data taken from Fig. 2 according to Equation 1 (full traces).

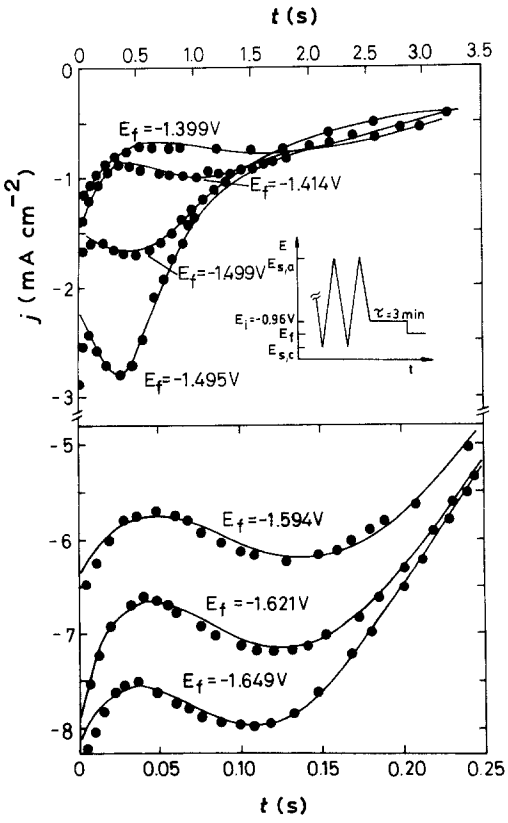

Fig. 10. Fitting of current transient data taken from Fig. 3 according to Equation 1 (full traces).

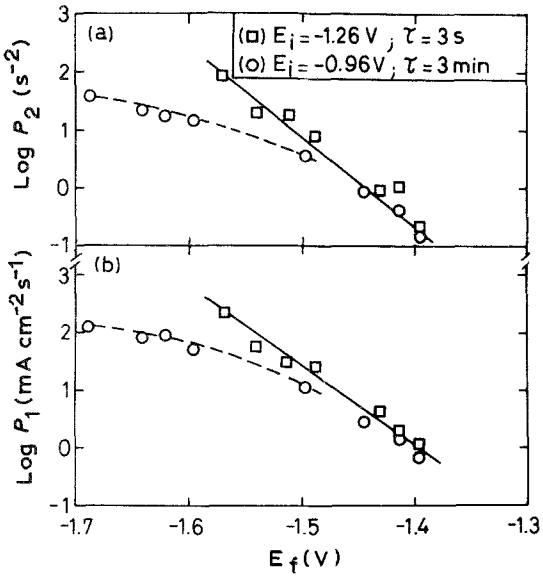

Fig. 11. Dependence of P_2(a) and P_1(b) on E_f. Data related to current transients depicted in Figs 9 (□) and 10 (○).

P_4 are explicitly given by the following relationships

$$P_3 = q_{mon}\pi K_i D_i N_0 \quad (6)$$

and

$$P_4 = \pi K_i D_i N_0 = P_3/q_{mon} \quad (7)$$

where K_i denotes a proportionally constant, $K_i = (8\pi c_i M\rho^{-1})^{1/2}$, D_i is the diffusion coefficient of the mobile species of concentration c_i involved in the process, and q_{mon} is the monolayer charge density. Alternatively, a relationship such as Equation 3 can also be assigned to an adsorption process, although under this circumstance the meanings of P_3 and P_4 are obviously different. Unfortunately, it is not possible at present to decide between these two reaction models exclusively on the basis of the satisfaction of Equation 3 in the initial portion of the potentiostatic current transients. The q_{mon} value resulting from the fitting procedure is about 0.5 ± 0.1 mC cm^{-2}.

Table 1. Parameters used for current transient fitting according to Equation 1 as shown in Figs 9 and 10 (full trace)

E_f (V)	P_1 (mA cm^{-2} s^{-1})	P_2 (s^{-2})	P_3 (mA cm^{-2})	P_4 (s^{-1})
E_i = −1.26 V	τ = 3 s			
−1.395	0.780	0.148	0.818	1.297
−1.416	2.027	1.256	5.811	0.693
−1.430	4.492	0.965	2.283	1.745
−1.493	24.570	8.681	0.910	5.235
−1.570	259.911	78.125	4.981	15.705
E_i = −0.96 V	τ = 3 min			
−1.399	0.684	0.152	1.317	2.550
−1.414	1.415	0.371	1.586	3.655
−1.495	12.377	3.754	3.431	10.377
−1.594	51.427	16.837	6.398	13.281
−1.621	67.524	20.876	7.662	15.833
−1.649	74.813	23.819	8.161	13.848
−1.688	124.964	40.663	10.954	21.836
−1.730	120.745	37.911	11.754	16.599

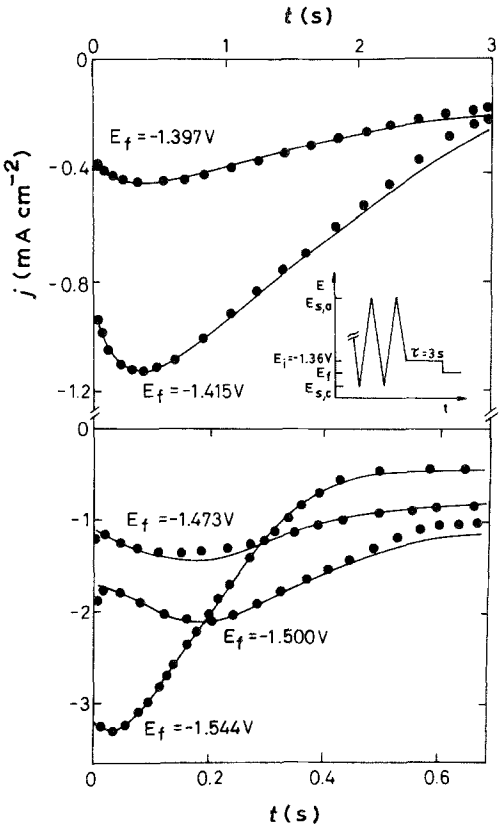

Fig. 12. Fitting of current transient data taken from Fig. 6 according to Equation 8 (full traces).

On the other hand, current decay resulting from the electroreduction of thicker anodic layers produced by anodization up to $E_{s,a}$ = −0.16 V (Fig. 6), can be described by the equation

$$j(t) = \frac{P_5}{t^{1/2}}[1 - \exp(-P_6 t)] + P_3 \exp(-P_4 t) \quad (8)$$

where the first term corresponds to an instantaneous nucleation and 3D growth under diffusion control, and the second term is as already given by Equation 3. Then, the current transients can be satifactorily reproduced (Fig. 12) through Equation 8, by taking

$$P_5 = \frac{zFD_j^{1/2}c_j}{\pi^{1/2}} \quad (9)$$

and

$$P_6 = \pi N_0 K_j D_j \quad (10)$$

and the fitting data assembled in Table 2. The dependence of P_3 and P_4 on the electroreduction potential is

Table 2. Parameters used for current transient fitting according to Equation 8 as shown in Fig. 12 (full trace)

E_f (V)	P_5 (mA cm^{-2} $s^{-1/2}$)	P_6 (s^{-1})	P_3 (mA cm^{-2})	P_4 (s^{-1})
E_i = −1.36 V	τ = 3 s			
−1.397	0.252	1.764	0.321	0.520
−1.415	0.745	2.222	0.604	0.800
−1.473	2.069	1.137	0.968	6.600
−1.500	3.073	1.166	1.911	8.420
−1.544	3.127	2.652	2.306	9.360
−1.560	1.090	7.446	2.725	5.303
−1.581	0.919	7.097	3.595	5.167

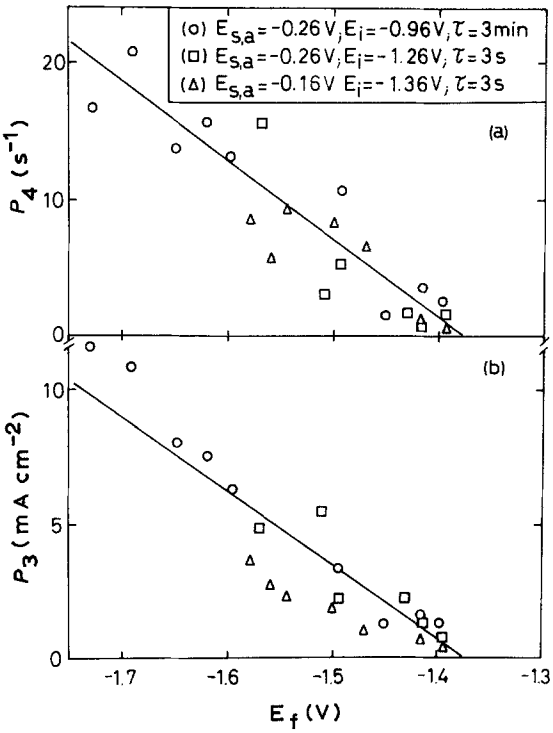

Fig. 13. Dependence of P_4(a) and P_3(b) on E_f. Data related to current transients depicted in Figs 9 (□), 10 (○), and 12 (△).

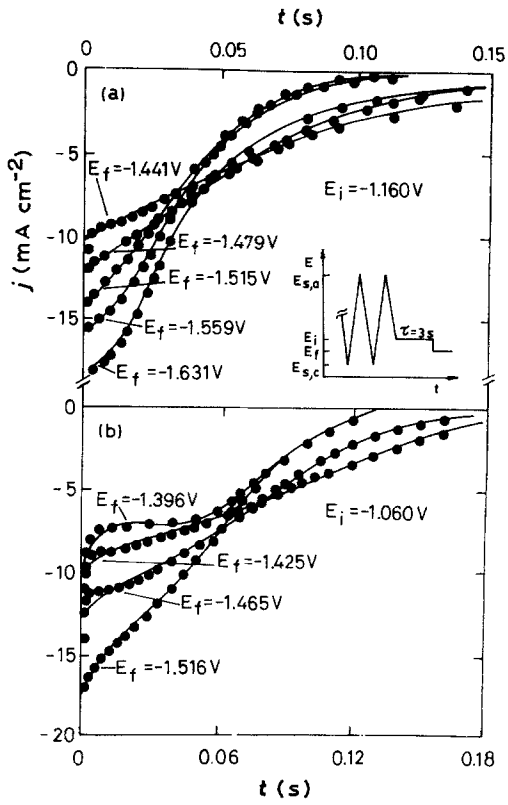

Fig. 14. Fitting of current transient data taken from Fig. 7 according to Equation 11 (full traces).

illustrated in Fig. 13 which also includes data displayed in Figs 2 and 3. The inspection of these results suggests that the instantaneous nucleation and 2D growth process under diffusion control prevails at short times.

The linear decrease of both P_3 and P_4 on increasing E_f positively, yields for P_i (i = 3, 4) $\Rightarrow$ 0, $E_f \simeq -1.37\,V \pm 0.020\,V$. The P_3/P_4 ratio reaches a q_{mon} value practically constant, $q_{mon} = 0.50 \pm 0.15\,mC\,cm^{-2}$, over a wide range of experimental conditions (Fig. 13). On the other hand, P_5 and P_6 become practically independent of E_f, having adjusted values close to $2.1 \pm 0.6\,mA\,cm^{-2}\,s^{-1/2}$ and $1.7 \pm 0.5\,s^{-1}$, respectively. By using for the CdS layer M = $144.5\,g\,mol^{-1}$ and $\rho = 4.8\,g\,cm^{-3}$ and assuming $c_j = 10^{-3}\,mol\,cm^{-3}$, one can estimate from Equation 9 the value of D_j which is about $3.7 \times 10^{-10}\,cm^2\,s^{-1}$. Under the present conditions the value of N_0 calculated from Equation 10 results in the order of 1.6×10^9 nuclei cm^{-2}.

4.2. *Thin CdS layer electroreduction mechanism*

The thin anodic layers produced by potential cycling up to $E_{s,a} = -0.86\,V$ (Fig. 14) can be attributed to the formation of one or two monolayers of CdS. Previous work [12, 13] has shown that the anodic peak A which is related to the initial stages of CdS film formation, involves two components whose relative contributions depend both on pH and Na_2S concentration in solution [13]. When these layers are held at E_i either $-1.16\,V$ (Fig. 7a) or $-1.06\,V$ (Fig. 7b), the cathodic current transients recorded at different E_f can be described by the expression

$$j(t) = P_3 \exp(-P_4 t) + P_7 t' \exp(-P_8 t'^2) \qquad (11)$$

The first term in Equation 11 corresponds to an instantaneous nucleation and 2D growth under diffusion control, similar to that expressed by Equations 3 and 8 and the second term corresponds to a progressive nucleation and 2D growth under diffusion control. The latter implies an induction time which is included in the time t'. The induction time is in the order of 1 ms. The parameters P_7 and P_8 are given by

$$P_7 = q'_{mon} \pi A K_k D_k \qquad (12)$$

and

$$P_8 = \pi A K_k D_k = P_7 / q'_{mon} \qquad (13)$$

where A denotes the nucleation rate constant ($s^{-1}\,cm^{-2}$) [21]. To demonstrate the quality of data fitting through Equation 13 (Fig. 14) the parameters P_7 and P_8 have been plotted as a function of E_f (Fig. 15). They fulfilled reasonable straight line relationships with E_f values extrapolated at P_i (i = 7, 8) $\longrightarrow$ 0 equal to $1.37 \pm 0.020\,V$, in agreement with that previously obtained for the P_i (i = 3, 4) against E_f plot (Fig. 13). Furthermore, the P_7/P_8 ratio yields a q'_{mon} value which is practically constant, $q'_{mon} \simeq 0.28 \pm 0.06\,mC\,cm^{-2}$.

5. Conclusions

The electroreduction kinetics of the anodic layers produced on Cd in Na_2S-containing alkaline solutions depend on whether the anodic layer was formed in the high or low potential range. In the high potential range an anodic layer composed of CdS and $Cd(OH)_2$ is obtained, whereas in the low potential range the

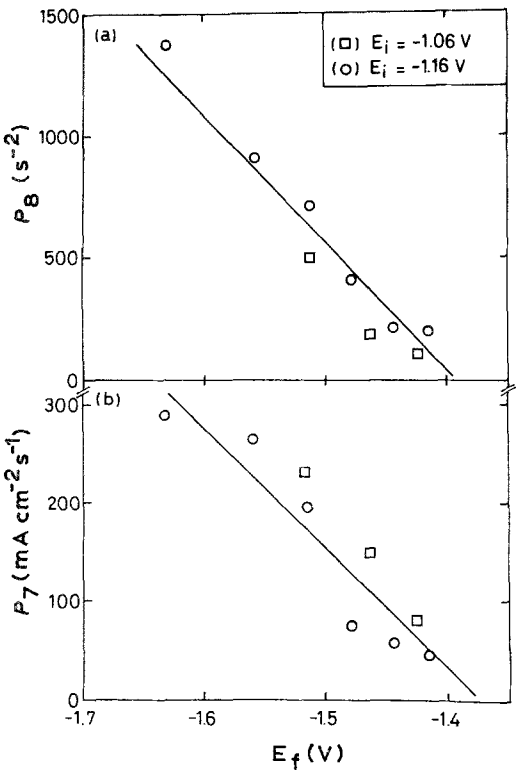

Fig. 15. Dependence of P_8(a) and P_7(b) on E_f. Data related to current transients depicted in Figs 14a (○) and 14b (□).

anodic layer is predominantly of CdS. In both cases the electroreduction process can be described through nucleation and growth kinetics under diffusion control.

The present results become, in principle, of interest for the electrochemical preparation of CdS electrodes of different thicknesses, and to know how the presence of cadmium oxide can influence the properties and stability of this type of electrode in relation to photoelectrochemical applications.

Acknowledgment

This research was financially supported by the Consejo Nacional de Investigaciones Científicas y Técnicas and the Comisión de Investigaciones Científicas de la Provincia de Buenos Aires.

References

[1] H. Gerischer, *Solar Energy Conversion* (edited by B. O. Sereaphin) Vol. 31, pp. 115–72, Springer-Verlag, Berlin (1979).
[2] A. Fujishima, K. Honda and K. Kohayakawa, *J. Electrochem. Soc.* **122** (1975) 1487.
[3] J. Janata, *Anal. Chim. Acta* **101** (1978) 239.
[4] T. Inoue, A. Fujishima and K. Honda, *J. Electrochem. Soc.* **127** (1980) 1582.
[5] H. Gerischer and J. Gobrecht, *Ber. Bunsenges* **82** (1978) 520.
[6] A. G. Stanley, *Applied Solid State Science*, Vol. 5, p. 251, Academic Press, New York (1979).
[7] B. Miller and A. Heller, *Nature* **262** (1976) 680.
[8] G. P. Power, D. R. Peggs and A. J. Parker, *Electrochim. Acta* **26** (1981) 681.
[9] B. Miller, S. Menezes and A. Heller, *J. Electroanal. Chem.* **94** (1978) 85.
[10] L. M. Peter, *Electrochim. Acta* **23** (1978) 165.
[11] L. S. R. Yeh, P. G. Hudson and A. Damjanovic, *J. Appl. Electrochem.* **12** (1953) 153.
[12] V. I. Birss and L. E. Kee, *J. Electrochem. Soc.* **133** (1986) 2097.
[13] S. B. Saidman, J. R. Vilche and A. J. Arvia, *Electrochim. Acta* **32** (1987) 1153.
[14] S. B. Saidman, M. López Teijelo, J. R. Vilche and A. J. Arvia, *An. Bras. Electroquim. Electroanal.* **4** (1986) 87.
[15] S. B. Saidman, J. R. Vilche and A. J. Arvia, *Thin Solid Films* **182** (1989) 185.
[16] Y. Okinaka, in 'Standard Potentials in Aqueous Solutions' (edited by A. J. Bard, R. Parson and J. Jordan), p. 257, Marcel Dekker, New York (1985).
[17] A. Gunawardena, G. J. Hills, I. Montenegro and B. R. Scharifker, *J. Electroanal. Chem.* **138** (1982) 225.
[18] M. Fleischmann and H. R. Thirsk, *J. Electrochem. Soc.* **110** (1963) 688.
[19] J. A. Harrison and H. R. Thirsk, in 'Advances in Electroanalytical Chemistry (edited by A. J. Bard), Vol. 5, p. 67, Marcel Dekker, New York (1971).
[20] H. R. Thirsk and J. A. Harrison, in 'A Guide to the Study of Electrode Kinetics', p. 121, Academic Press, New York (1972).
[21] B. R. Scharifker and J. Mostany, *J. Electroanal. Chem.* **177** (1984) 13.
[22] R. D. Armstrong and J. A. Harrison, *J. Electrochem. Soc.* **116** (1969) 328.